JOURNAL OF COMPUTATIONAL PHYSICS 104, 251–262 (1993)

Numerical Mapping of Arbitrary Domains Using Spectral Methods

G. P. KOOMULLIL AND Z. U. A. WARSI*

Department of Aerospace Engineering, Mississippi State University, Mississippi State, Mississippi 39762

Received August 29, 1990; revised March 27, 1992

In order to maintain spectral accuracy, the grids on which a physical problem is to be solved must also be obtained by spectrally accurate techniques. The purpose of this paper is to describe a method of solving the quasilinear elliptic grid generation equations by spectral techniques both in Euclidean (E^2) and Riemannian (R^2) spaces. A parametric continuation method is used to generate grids in completely arbitrary domains.

I. INTRODUCTION

In recent times there is much interest in the use of spectral methods for the solution of physical problems involving nonlinear partial differential equations. This trend is more evident in the area of computational fluid dynamics where, in some cases, highly accurate solutions are needed to resolve the flow field. Practical finite difference methods by their very nature can provide solutions to a certain order of accuracy which may not be sufficient in the computations of some flows, e.g., transitional flows and simulated turbulent flows. In contrast, the spectral methods provide a capability of obtaining rapidly convergent solutions, with a further advantage of practically no dissipation errors. A monograph by Gottlieb and Orszag [1] and a recent book by Canuto *et al.* [2] provide a thorough grounding in the state of the art of the spectral methods.

The main thrust of the spectral methods has been inhibited due to a lack of their application to field problems involving complicated geometries. Most of the problems which have been solved by using spectral methods have usually been restricted to simple geometries. In some difficult geometries, the domain decomposition method has been used, Ref. [2]. A fairly general and automatic method of numerical mapping technique is needed which can maintain the same level of accuracy as the accuracy of the method used in solving the physical problem, e.g., the Navier–Stokes equations. In this context, it is important to point out that when solving a physical problem on a complicated geometry, the transformed physical equations require a knowledge of various partial derivatives, metric coefficients, etc. of the coordinate system. Since these quantities must also be computed with spectral accuracy, the available numerical mapping techniques used in the finite difference solutions cannot be used for spectral solutions. Thus, as was first pointed out by Orszag [3], a computational procedure to generate coordinates is needed which is capable of maintaining spectral accuracy. The order of accuracy problem has been addressed by Koomullil in an exhaustive manner [4].

It is the purpose of this paper to develop the necessary methodology for generating curvilinear coordinates for arbitrary domains in two- and three-dimensional Euclidean E^2 and E^3 spaces and also in two-dimensional surfaces embedded in E^3 space, i.e., R^2-space. The method is based on the elliptic partial differential equations of the Poisson's type [5, 6]. Since this transformation technique leads to quasilinear PDEs, a proper method has to be developed to overcome the problem of non-constant coefficients. In this research it has been shown that a "parametric continuation method" as advocated by Keller [7] coupled with a time stepping scheme works quite efficiently. Among the various time stepping schemes the simplest, due to Euler, has been adopted in this paper.

Numerical grids have been generated using appropriate spectral methods for a variety of simply and doubly connected domains in E^2 and in simply connected domains in R^2, using the equations proposed by Warsi [8]. Generation of coordinates in E^3 seems to be a direct extension, although with more computational and programming effort. In this paper, a general formulation of grid generation using elliptic partial differential equations, including all the forcing functions, has been given, e.g., refer to [9]. However, to demonstrate the use of spectral methods for generating grids we have considered only the case when all

* The first author acknowledges the award of a graduate assistantship while the second author acknowledges partial support of this research from the NSF Engineering Research Center at the Mississippi State University.

0021-9991/93 $5.00

the forcing functions are set to zero. Even if the control functions are not set to zero, the grids generated by spectral methods will be spectrally accurate. Though it has not been reported here, the authors have studied the effect of control functions and have found that a desired distribution of collocation points in the logical plane can be obtained by choosing appropriate control functions without any decrease of grid smoothness. These topics are beyond the intent and purpose of this paper and, therefore, the results concerning the use of control functions, grid resolution, and the important topic of the accuracy needed for the calculation of the metric coefficients in relation to the accuracy of the Navier–Stokes solutions will form the subject of a future paper.

II. GRID GENERATION

In this section, we briefly summarize the elliptic grid generation equations both for the three-dimensional Euclidean space (E^3) and the two-dimensional Riemannian space (R^2). The grid generation equations are taken as a set of time-dependent Poisson's equations in E^3 and the Laplace/Beltrami equations in R^2. As has been discussed in the Introduction, the purpose of adopting the time-dependent grid generation equations is not to solve for time-accurate coordinate systems but to develop a *parametric continuation* method (refer to Keller [7] and the references therein) for applying the spectral technique to generate grids for arbitrarily shaped bodies. Thus, in the context of the *parametric continuation* method, a parameter σ as defined below is considered as the continuation parameter. The aim is to use a time stepping numerical procedure to drive the solution to a state of parametric independency, or, towards a steady state.

For the purpose of model development, we shall use the suffix notation (refer to Appendix B for definitions). As has been shown in various publications, e.g., [9, 6], the elliptic grid generation equations in the transformed plane both in E^2 and E^3 stem from the vector equation

$$g^{ij}\mathbf{r}_{,ij} + (\nabla^2 x^k)\,\mathbf{r}_{,k} = 0, \tag{2.1}$$

where $\mathbf{r} = (x, y, z)$. We now take the elliptic grid generation equations as a set of time-dependent Poisson's equations

$$\nabla^2 x^k = g^{ij}P^k_{ij} + \frac{c}{g}\frac{\partial x^k}{\partial t}, \tag{2.2}$$

where $g = \det(g_{ij})$, P^k_{ij} are the user specified control functions, and a dimensional constant c has been introduced so as to have non-dimensional curvilinear coordinates. Substituting (2.2) in Eq. (2.1), we obtain

$$\mathscr{L}\mathbf{r} + c\mathbf{r}_{,k}\frac{\partial x^k}{\partial t} = 0, \tag{2.3a}$$

where the operator $\mathscr{L}$ is

$$\mathscr{L} = D + gg^{ij}P^k_{ij}\frac{\partial}{\partial x^k},$$
$$D = gg^{ij}\frac{\partial^2}{\partial x^i\,\partial x^j}. \tag{2.3b}$$

For non-steady coordinates

$$x^k = x^k(\mathbf{r}, t), \quad \tau = t,$$

and

$$\mathbf{r} = \mathbf{r}(x^k, \tau), \quad t = \tau.$$

Following the analysis given in [10], we have

$$\frac{\partial \mathbf{r}}{\partial \tau} = -\mathbf{w} = -\mathbf{r}_{,k}\frac{\partial x^k}{\partial t}. \tag{2.3c}$$

Using (2.3c) in Eq. (2.3a) and writing $\sigma = \tau/c$, we finally have

$$\frac{\partial \mathbf{r}}{\partial \sigma} = \mathscr{L}\mathbf{r}, \tag{2.4}$$

which are three equations in E^3 for $\mathbf{r} = (x, y, z)$ and two equations in E^2 for $\mathbf{r} = (x, y)$.

Writing $x^1 = \xi$, $x^2 = \eta$, $x^3 = \zeta$, and

$$g^{11} = G_1/g, \quad g^{22} = G_2/g, \quad g^{33} = G_3/g,$$
$$g^{12} = G_4/g, \quad g^{13} = G_5/g, \quad g^{23} = G_6/g,$$

we have

$$\mathscr{L} = G_1\partial_{\xi\xi} + G_2\partial_{\eta\eta} + G_3\partial_{\zeta\zeta} + 2G_4\partial_{\xi\eta} + 2G_5\partial_{\xi\zeta} + 2G_6\partial_{\eta\zeta} + P^1\partial_\xi + P^2\partial_\eta + P^3\partial_\zeta, \tag{2.5a}$$

where, for $k = 1, 2, 3$,

$$P^k = G_1P^k_{11} + G_2P^k_{22} + G_3P^k_{33} + 2G_4P^k_{12} + 2G_5P^k_{13} + 2G_6P^k_{23}. \tag{2.5b}$$

Both (2.5a), (2.5b) are greatly simplified for the two-dimensional (E^2) case in which

$$G_1 = g_{22}, \quad G_2 = g_{11}, \quad G_3 = g_{11}\,g_{22} - (g_{12})^2 = g,$$

$$G_4 = -g_{12}, \quad G_5 = 0, \quad G_6 = 0,$$

and the derivatives with respect to ζ are zero.

For a curved surface embedded in E^3 the space is R^2 in which, as shown by Warsi [8], the basic equations stem from

$$g^{\alpha\beta}\mathbf{r}_{,\alpha\beta} + (\Delta_2^{(\nu)}x^\delta)\,\mathbf{r}_{,\delta} = (k_I^{(\nu)} + k_{II}^{(\nu)})\,\mathbf{n}^{(\nu)}, \tag{2.6}$$

where the superscript (ν) means the surface $x^\nu = \text{const}$. In general, the Laplace/Beltrami equations taken as coordinate generators are taken as

$$\Delta_2^{(\nu)}x^\delta = g^{\alpha\beta}P^\delta_{\alpha\beta} + \frac{c}{G_\nu}\frac{\partial x^\delta}{\partial t}. \tag{2.7}$$

Since the two-dimensional Riemannian space is embedded in E^3 and one of the coordinates $x^\nu = \text{const}$, then

$$\frac{\partial \mathbf{r}}{\partial \tau} = -\mathbf{w} = -\mathbf{r}_{,\delta}\frac{\partial x^\delta}{\partial t}. \tag{2.8}$$

Introducing (2.7) and (2.8) in Eq. (2.6), we obtain

$$\frac{\partial \mathbf{r}}{\partial \sigma} = \mathscr{L}\mathbf{r} - \mathbf{n}^{(\nu)}R, \tag{2.9}$$

where

$$\mathscr{L} = D + G_\nu g^{\alpha\beta}P^\delta_{\alpha\beta}\frac{\partial}{\partial x^\delta},$$

$$D = G_\nu g^{\alpha\beta}\frac{\partial^2}{\partial x^\alpha\,\partial x^\beta},$$

$$R = (k_I^{(\nu)} + k_{II}^{(\nu)})\,G_\nu,$$

$$\sigma = \tau/c.$$

Equation (2.9) represents three equations each for x, y, and z. In particular, for $\nu = 3$, i.e., $x^3 = \text{const}$, writing $x^1 = \xi$, $x^2 = \eta$, and noting that

$$G_3 = g_{11}\,g_{22} - (g_{12})^2$$

$$g^{11} = g_{22}/G_3, \quad g^{12} = -g_{12}/G_3, \quad g^{22} = g_{11}/G_3,$$

we obtain

$$\mathscr{L} = g_{22}\partial_{\xi\xi} - 2g_{12}\partial_{\xi\eta} + g_{11}\partial_{\eta\eta} + P^1\partial_\xi + P^2\partial_\eta, \tag{2.10a}$$

$$P^1 = g_{22}P^1_{11} - 2g_{12}P^1_{12} + g_{11}P^1_{22},$$
$$P^2 = g_{22}P^2_{11} - 2g_{12}P^2_{12} + g_{11}P^2_{22}. \tag{2.10b}$$

Note that in (2.10) the metric coefficients depend on all three physical coordinates x, y, and z, i.e.,

$$g_{\alpha\beta} = \mathbf{r}_{,\alpha}\cdot\mathbf{r}_{,\beta}.$$

To incorporate the capability of one-dimensional control along the coordinate lines, the control functions of the form P^k_{kk} (no summation on k) in either (2.5b) or (2.10b) are retained and the rest of them are set equal to zero. This is what has been done in this paper.

III. SPECTRAL FORMULATION

In this section, we formulate the problem of solving the grid generation equations, either Eq. (2.4) or Eq. (2.9), by using spectral methods. The choice of the global basis functions in the spectral expansions is dictated by the nature of the domain in which the grids are to be generated. Thus, for a simply connected domain, both in E^2 and R^2, the choice of the basis functions as Chebyshev polynomials $T_n(x)$ seems to be a judicious one. On the other hand, for doubly connected domains, a Fourier–Chebyshev expansion is desirable due to the periodicity requirement on one coordinate. In the following analysis, we have used a number of recursive and derivative formulas involving the Chebyshev polynomials. All such formulas have been collected in Appendix A. Below, we have considered the formulations of simply connected domains in E^2 and R^2 and of doubly connected domains in E^2.

Case I. Simply connected domain in E^2. We normalize the coordinates ξ and η to the range $(-1, 1)$ and write the spectral expansion of $\mathbf{r} = (x, y)$ as

$$\mathbf{r}(\xi, \eta) = \sum_{m=0}^{M}\sum_{n=0}^{N}\mathbf{a}^{(0)(0)}_{mn}T_m(\xi)\,T_n(\eta),$$

$$-1 \leqslant \xi \leqslant 1, -1 \leqslant \eta \leqslant 1. \tag{3.1}$$

Using Eqs. (A.14) and (A.15) for the derivatives, we have

$$\mathbf{r}_\xi = \sum_{m=0}^{M}\sum_{n=0}^{N} \mathbf{a}_{mn}^{(1)(0)} T_m(\xi)\, T_n(\eta),$$

$$\mathbf{r}_\eta = \sum_{m=0}^{M}\sum_{n=0}^{N} \mathbf{a}_{mn}^{(0)(1)} T_m(\xi)\, T_n(\eta),$$

$$\mathbf{r}_{\xi\xi} = \sum_{m=0}^{M}\sum_{n=0}^{N} \mathbf{a}_{mn}^{(2)(0)} T_m(\xi)\, T_n(\eta),$$

$$\mathbf{r}_{\eta\eta} = \sum_{m=0}^{M}\sum_{n=0}^{N} \mathbf{a}_{mn}^{(0)(2)} T_m(\xi)\, T_n(\eta),$$

$$\mathbf{r}_{\xi\eta} = \sum_{m=0}^{M}\sum_{n=0}^{N} \mathbf{a}_{mn}^{(1)(1)} T_m(\xi)\, T_n(\eta), \tag{3.2}$$

$$\mathbf{a}_{mn}^{(1)(0)} = \frac{2}{c_m} \sum_{\substack{p=m+1 \\ p+m \text{ odd}}}^{M} p\,\mathbf{a}_{pn}^{(0)(0)},$$

$$\mathbf{a}_{mn}^{(0)(1)} = \frac{2}{c_n} \sum_{\substack{q=n+1 \\ q+n \text{ odd}}}^{N} q\,\mathbf{a}_{mq}^{(0)(0)},$$

$$\mathbf{a}_{mn}^{(2)(0)} = \frac{1}{c_m} \sum_{\substack{p=m+2 \\ p+m \text{ even}}}^{M} p(p^2-m^2)\,\mathbf{a}_{pn}^{(0)(0)},$$

$$\mathbf{a}_{mn}^{(0)(2)} = \frac{1}{c_n} \sum_{\substack{q=n+2 \\ q+n \text{ even}}}^{N} q(q^2-n^2)\,\mathbf{a}_{mq}^{(0)(0)},$$

$$\mathbf{a}_{mn}^{(1)(1)} = \frac{4}{c_m c_n} \sum_{\substack{q=n+1 \\ q+n \text{ odd}}}^{N} \sum_{\substack{p=m+1 \\ p+m \text{ odd}}}^{M} pq\,\mathbf{a}_{pq}^{(0)(0)}. \tag{3.3}$$

As noted in Appendix A, $c_0 = 2$, $c_r = 1$ for $r > 0$.

We now take the metric coefficients as depending on the previously computed coefficients a_{mn}, and further that they are constants in each sweep and having the values $g_{ij}(\xi_m, \eta_n)$. With this stipulation using (4.2) in Eqs. (3.4) and (A.12), we have

$$\frac{\partial \mathbf{a}_{mn}^{(0)(0)}}{\partial \sigma} = \hat{\mathscr{L}}(\mathbf{a}_{mn}^{(0)(0)}), \tag{3.4}$$

where

$$\hat{\mathscr{L}}(\mathbf{a}_{mn}^{(0)(0)}) = \frac{g_{22}}{c_m}\Bigg[\sum_{\substack{p=m+2 \\ p+m \text{ even}}}^{M} p(p^2-m^2)\,\mathbf{a}_{pn}^{(0)(0)} + 2P_{11}^{1} \sum_{\substack{p=m+1 \\ p+m \text{ odd}}}^{M} p\,\mathbf{a}_{pn}^{(0)(0)} \Bigg] - \frac{8g_{12}}{c_m c_n} \sum_{\substack{q=n+1 \\ q+n \text{ odd}}}^{N} \sum_{\substack{p=m+1 \\ p+m \text{ odd}}}^{M} pq\,\mathbf{a}_{pq}^{(0)(0)} + \frac{g_{11}}{c_n}\Bigg[\sum_{\substack{q=n+2 \\ q+n \text{ even}}}^{N} q(q^2-n^2)\,\mathbf{a}_{mq}^{(0)(0)} + 2P_{22}^{2} \sum_{\substack{q=n+1 \\ q+n \text{ odd}}}^{N} q\,\mathbf{a}_{mq}^{(0)(0)} \Bigg]. \tag{3.5}$$

Using forward Euler's method, the parameter-stepping is achieved by discretizing (3.4) as

$$\mathbf{a}_{mn}^{(0)(0)}(\sigma + \Delta\sigma) = \mathbf{a}_{mn}^{(0)(0)}(\sigma) + \Delta\sigma\, \hat{\mathscr{L}}(\mathbf{a}_{mn}^{(0)(0)}(\sigma)), \tag{3.6}$$

where the last term in (3.6) is evaluated through (3.5) by using the values of g_{11}, g_{12}, and g_{22} as available at σ. For the actual implementation[1] of (3.6) and on the use of other explicit methods, refer to Section IV.

Case II. Doubly connected domain in E^2. In a doubly connected domain, we use the Fourier–Chebyshev expansion as

$$\mathbf{r}(\xi, \eta) = \sum_{m=-M/2}^{M/2-1} \sum_{n=0}^{N} \mathbf{a}_{mn}^{(0)(0)} e^{im\xi} T_n(\eta), \tag{3.7}$$

where now $0 \leqslant \xi \leqslant 2\pi$, $-1 \leqslant \eta \leqslant 1$, and $i = \sqrt{-1}$. Again using Eqs. (A.14) and (A.15), we have

$$\mathbf{a}_{mn}^{(0)(1)} = \frac{2}{c_n} \sum_{\substack{q=n+1 \\ q+n \text{ odd}}}^{N} q\,\mathbf{a}_{mn}^{(0)(0)},$$

$$\mathbf{a}_{mn}^{(0)(2)} = \frac{1}{c_n} \sum_{\substack{q=n+2 \\ q+n \text{ even}}}^{N} q(q^2-n^2)\,\mathbf{a}_{mq}^{(0)(0)}, \tag{3.8}$$

$$\mathbf{a}_{mn}^{(1)(1)} = im\,\frac{2}{c_n} \sum_{\substack{q=n+1 \\ q+n \text{ odd}}}^{N} q\,\mathbf{a}_{mq}^{(0)(0)},$$

[1] It is implicitly understood that all the coefficients appearing above and in the succeeding equations are the discrete coefficients as defined in Section IV.

while the following are obvious:

$$\mathbf{a}_{mn}^{(1)(0)} = im\mathbf{a}_{mn}^{(0)(0)},$$
$$\mathbf{a}_{mn}^{(2)(0)} = -m^2\mathbf{a}_{mn}^{(0)(0)}.$$

Substitution of the various derivatives of (3.7) in Eq. (2.4) results in the following expression for $\hat{\mathscr{L}}(\cdots)$:

$$\hat{\mathscr{L}}(\mathbf{a}_{mn}^{(0)(0)}) = g_{22}(-m^2\mathbf{a}_{mn}^{(0)(0)} + imP_{11}^1\mathbf{a}_{mn}^{(0)(0)}) - \frac{4g_{12}}{c_n}\left[im \sum_{\substack{q=n+1 \\ q+n \text{ odd}}}^{N} q\mathbf{a}_{mq}^{(0)(0)}\right] + \frac{g_{11}}{c_n}\left[\sum_{\substack{q=n+2 \\ q+n \text{ even}}}^{N} q(q^2-n^2)\,\mathbf{a}_{mq}^{(0)(0)} + 2P_{22}^2 \sum_{\substack{q=n+1 \\ q+n \text{ odd}}}^{N} q\mathbf{a}_{mq}^{(0)(0)}\right].$$

Writing

$$\mathbf{a}_{mn} = \mathbf{A}_{mn} + i\mathbf{B}_{mn},$$

and noting that g_{11}, g_{12}, g_{22}, P_{11}^1, and P_{22}^2 are real, we obtain

$$\frac{\partial \mathbf{A}_{mn}^{(0)(0)}}{\partial\sigma} = g_{22}[-m^2\mathbf{A}_{mn}^{(0)(0)} - mP_{11}^1\mathbf{B}_{mn}^{(0)(0)}] + 4\frac{g_{12}}{c_n}\left[m \sum_{\substack{q=n+1 \\ q+n \text{ odd}}}^{N} q\mathbf{B}_{mq}^{(0)(0)}\right] + \frac{g_{11}}{c_n}\left[\sum_{\substack{q=n+2 \\ q+n \text{ even}}}^{N} q(q^2-n^2)\,\mathbf{A}_{mq}^{(0)(0)} + 2P_{22}^2 \sum_{\substack{q=n+1 \\ q+n \text{ odd}}}^{N} q\mathbf{A}_{mq}^{(0)(0)}\right] \tag{3.9}$$

$$\frac{\partial \mathbf{B}_{mn}^{(0)(0)}}{\partial\sigma} = g_{22}[-m^2\mathbf{B}_{mn}^{(0)(0)} + mP_{11}^1\mathbf{A}_{mn}^{(0)(0)}] - 4\frac{g_{12}}{c_n}\left[m \sum_{\substack{q=n+1 \\ q+n \text{ odd}}}^{N} q\mathbf{A}_{mq}^{(0)(0)}\right] + \frac{g_{11}}{c_n}\left[\sum_{\substack{q=n+2 \\ q+n \text{ even}}}^{N} q(q^2-n^2)\,\mathbf{B}_{mq}^{(0)(0)} + 2P_{22}^2 \sum_{\substack{q=n+1 \\ q+n \text{ odd}}}^{N} q\mathbf{B}_{mq}^{(0)(0)}\right], \tag{3.10}$$

where, as has been noted earlier, only the control functions P_{11}^1 and P_{22}^2 have been retained. Equations (3.9) and (3.10) are solved by the parameter-stepping method similar to (3.6).

Case III. Simply connected domain in R^2. Applications of the spectral technique to Eq. (2.9) for the generation of coordinates in a given surface $F(x, y, z) = 0$ requires additional considerations due to the appearance of the terms $\mathbf{n}$ and R, [11]. The quantity R depends on the function $F(x, y, z) = 0$ and the value of R/G_3 is computed by using the formula given in [8, Eq. (4.1)]. On the other hand, the unit normal vector $\mathbf{n}$ is given as

$$\mathbf{n} = (\mathbf{r}_\xi \times \mathbf{r}_\eta)/\sqrt{G_3}.$$

Thus, proceeding from

$$\mathbf{r}(\xi, \eta) = \sum_{r=0}^{M}\sum_{s=0}^{N} \mathbf{a}_{rs}^{(0)(0)} T_r(\xi)\, T_s(\eta),$$

we obtain

$$\mathbf{n} = \frac{1}{4\sqrt{G_3}} \sum_{r=0}^{M}\sum_{s=0}^{N}\sum_{p=0}^{M}\sum_{q=0}^{N} \mathbf{d}_{rspq} T_{r+p}(\xi)\, T_{s+q}(\eta) + T_{r+p}(\xi)\, T_{s-q}(\eta) + T_{r-p}(\xi)\, T_{s+q}(\eta) + T_{r-p}(\xi)\, T_{s-q}(\eta), \tag{3.11}$$

where the components of the vector $\mathbf{d}_{rspq}$, defined by

$$\mathbf{d}_{rspq} = \mathbf{a}_{rs}^{(1)(0)} \times \mathbf{a}_{pq}^{(0)(1)}$$

are

$$\mathbf{d}_{rspq}(j) = \mathbf{a}_{rs}^{(1)(0)}(k)\, \mathbf{a}_{pq}^{(0)(1)}(l) - \mathbf{a}_{rs}^{(1)(0)}(l)\, \mathbf{a}_{pq}^{(0)(1)}(k),$$

with j, k, l in this order, are the cyclic permutations of 1, 2, 3.

Manipulation of terms in (3.11) finally yields

$$\mathbf{n} = \frac{1}{4\sqrt{G_3}} \sum_{m=0}^{M}\sum_{n=0}^{N} \mathbf{A}_{mn} T_m(\xi)\, T_n(\eta), \tag{3.12}$$

where

$$\mathbf{A}_{mn} = \sum_{p=0}^{M} \left[\sum_{q=0}^{N} \mathbf{d}_{pq}(|p-m|)(|q-n|) + \sum_{q=0}^{N-n} \mathbf{d}_{pq}(|p-m|)(q+n) \right] + \sum_{p=0}^{M-m} \left[\sum_{q=0}^{N} \mathbf{d}_{pq}(p+m)(|q-n|) + \sum_{q=0}^{N-n} \mathbf{d}_{pq}(p+m)(q+n) \right].$$

IV. NUMERICAL IMPLEMENTATION

The grid generation equations (Eq. (2.4) or Eq. (2.9)) can be integrated by any of the explicit time or parameter stepping schemes. For solving Eq. (2.4), we have used the forward Euler, second-order Adams–Bashforth, and the fourth-order Runge–Kutta schemes. It has been found that for the problems of grid generation under consideration the forward Euler scheme is the scheme of choice. To demonstrate the trend of error decrement, we chose the problem of grid generation between two concentric ellipses; the larger one having semi-major and minor axes twice that of the smaller. Figure 1 shows the error E defined as

$$E = \sum_{i=0}^{M} \sum_{j=0}^{N} \{|x_{ij}^{n+1} - x_{ij}^{n}| + |y_{ij}^{n+1} - y_{ij}^{n}|\}, \quad (4.1a)$$

with the parameter index number n. In this study, the maximum allowable parameter step as well as the minimum computational time and effort were found to be with the forward Euler scheme. Hence, in all other examples, we have used the forward Euler method for time integration. The error in surface grid generation is defined by

$$E = \sum_{i=0}^{M} \sum_{j=0}^{N} \{|x_{ij}^{n+1} - x_{ij}^{n}| + |y_{ij}^{n+1} - y_{ij}^{n}| + |z_{ij}^{n+1} - z_{ij}^{n}|\} \quad (4.1b)$$

As is shown by Eq. (3.6), the parameter-stepping is carried out in the spectral space and therefore, it becomes necessary to obtain the imposed boundary conditions in terms of the spectral coefficients. First, the boundary values have to be written spectrally as

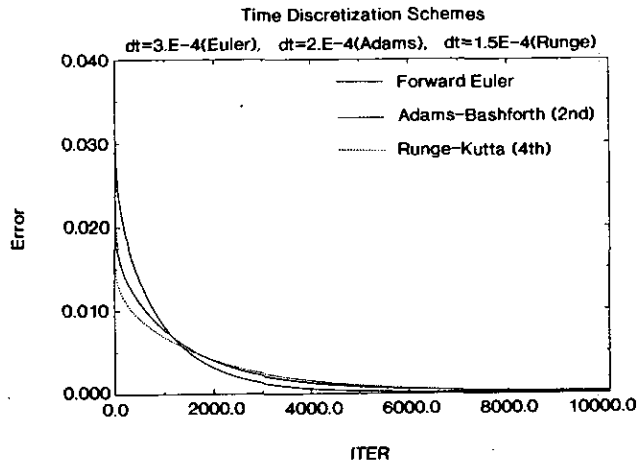

FIG. 1. Comparison of error decrement trends using various time stepping techniques.

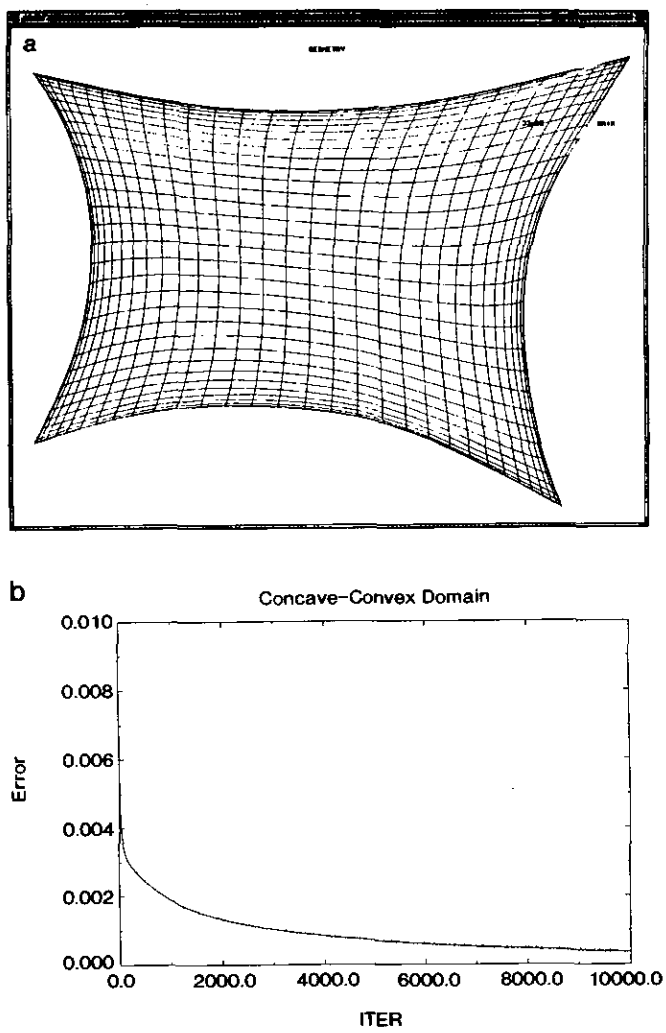

FIG. 2. (a) Simply connected domain bounded by arbitrary concave convex curves. (b) Error decrement behavior in the parameter stepping procedure used in obtaining the coordinates in Fig. 2a.

$$\mathbf{r}(\xi,-1)=\sum_m \mathbf{a}_m T_m(\xi),$$

$$\mathbf{r}(\xi,1)=\sum_m \mathbf{e}_m T_m(\xi),$$

$$\mathbf{r}(-1,\eta)=\sum_n \mathbf{d}_n T_n(\eta),$$

$$\mathbf{r}(1,\eta)=\sum_n \mathbf{b}_n T_n(\eta). \tag{4.1c}$$

Thus, using (3.1), we arrive at the equations

$$\sum_n \mathbf{a}_{mn}^{(0)(0)}(-1)^n=\mathbf{a}_m,$$

$$\sum_n \mathbf{a}_{mn}^{(0)(0)}=\mathbf{e}_m,$$

$$\sum_m \mathbf{a}_{mn}^{(0)(0)}(-1)^m=\mathbf{d}_n,$$

$$\sum_m \mathbf{a}_{mn}^{(0)(0)}=\mathbf{b}_n. \tag{4.1d}$$

This procedure produces an underdetermined problem, viz., it involves the solution of $4(M+1)+4(N+1)$ scalar equations for $2(M+1)\times(N+1)$ scalar unknowns. In view of this problem, we adopt a different procedure in which the spectral coefficients are transformed back to the physical space (refer to Eq. (4.2a)) and then the boundary conditions are imposed. For the purpose of comparing the computed coefficients with the coefficients of the underdetermined system we first use the coefficients $\mathbf{a}_{mn}^{(0)(0)}$ in Eqs. (4.1d) to calculate $\mathbf{a}_m$, $\mathbf{e}_m$, $\mathbf{d}_n$, and $\mathbf{b}_n$. Next the transform of Eqs. (4.1c) is taken and the calculated coefficients are denoted as $\mathbf{p}_m$, $\mathbf{q}_m$, $\mathbf{r}_n$, and $\mathbf{s}_n$. The differences

$$\mathbf{a}_m-\mathbf{p}_m,\quad \mathbf{e}_m-\mathbf{q}_m,\quad \mathbf{d}_n-\mathbf{r}_n,\ \mathbf{b}_n-\mathbf{s}_n$$

are then formed, and it has been found that the absolute sum of these errors for the whole boundary, e.g.,

$$\sum_{m=0}^{M}|\mathbf{a}_m-\mathbf{p}_m|$$

is less than 10^{-8}. These small differences are due to the single precision transforms used to obtain the coefficients.

To summarize the complete numerical procedure, we first state the discrete Chebyshev transform pair for two-dimensional domains. Refer to [2] for a basic understanding of the technique. The discrete Chebyshev transform pair based on the Gauss–Lobatto points for simply connected domains is

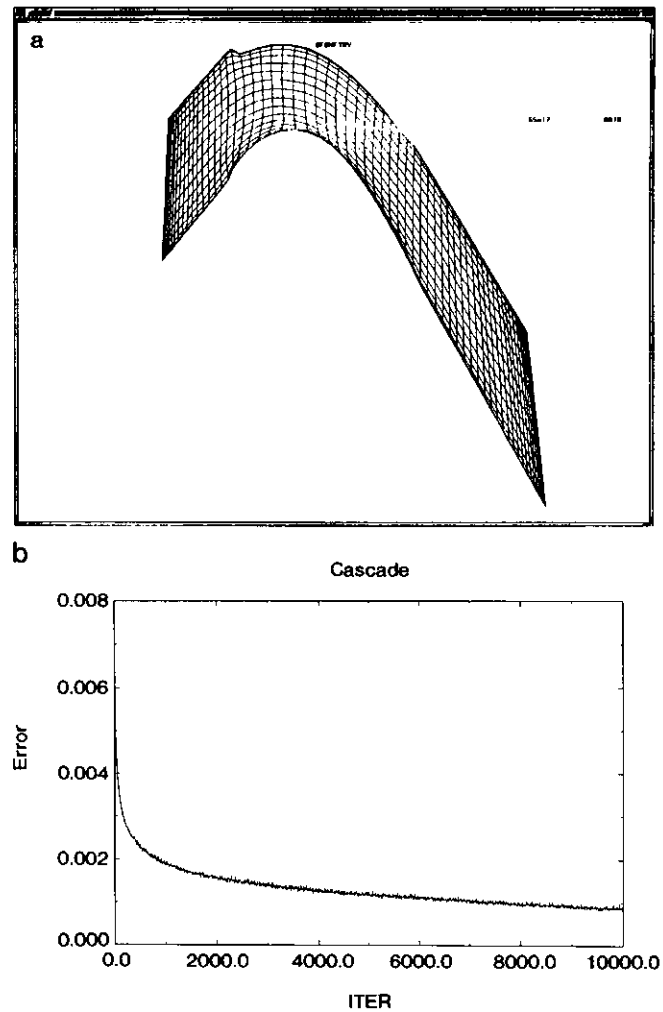

FIG. 3. (a) Coordinates generated in a gas turbine rotor blade. (b) Error decrement behavior inthe parameter stepping procedure used in obtaining the coordinates in Fig. 3a.

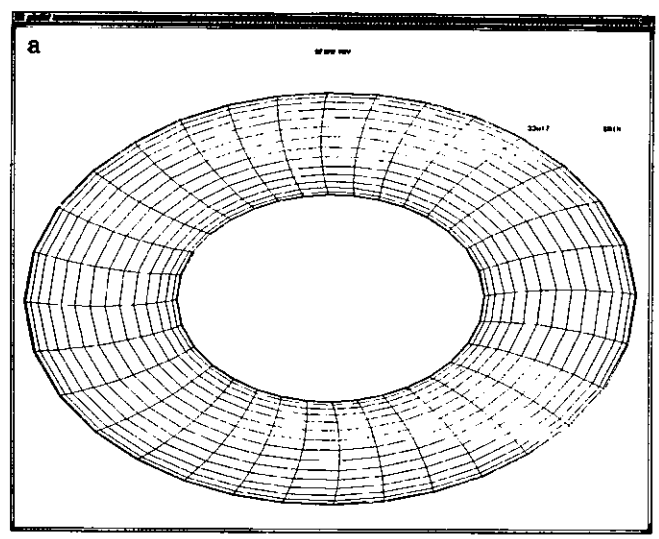

FIG. 4. Coordinates generated between two ellipses. Minor and major axes ratio of 2:1.

$$\mathbf{r}_{jk} = \sum_{m=0}^{M} \sum_{n=0}^{N} \hat{\mathbf{a}}_{mn}^{(0)(0)} \cos\frac{\pi jm}{M} \cos\frac{\pi kn}{N}, \tag{4.2a}$$

$$j = 1, 2, ..., M-1; k = 1, 2, ..., N-1,$$

$$\hat{\mathbf{a}}_{mn}^{(0)(0)} = \frac{4}{MN\bar{c}_m\bar{c}_n} \sum_{j=0}^{M} \sum_{k=0}^{N} \frac{1}{\bar{c}_j\bar{c}_k} \mathbf{r}_{jk} \cos\frac{\pi jm}{M} \cos\frac{\pi kn}{N}, \tag{4.2b}$$

where

$$m = 0, 1, ..., M; n = 0, 1, ..., N,$$

and

$$\bar{c}_j = 2 \quad \text{if} \quad j = 0 \text{ or } M,$$
$$= 1 \quad \text{if} \quad 1 \leqslant j \leqslant M-1,$$
$$\bar{c}_k = 2 \quad \text{if} \quad k = 0 \text{ or } N,$$
$$= 1 \quad \text{if} \quad 1 \leqslant k \leqslant N-1.$$

Here $\hat{\mathbf{a}}_{mn}^{(0)(0)}$ are the discrete spectral coefficients. For doubly connected regions, one of the coordinates is periodic and, therefore, a Fourier–Chebyshev expansion has been used. In any event, one complete iteration uses both Eqs. (4.2a) and (4.2b); first to solve the discretized equations in the spectral space and next to impose the boundary conditions in the physical space.

To start the iteration procedure, we need the initial variables at the quadrature nodes. In the present problems, the quadrature nodes taken for the Chebyshev polynomials are the Gauss–Lobatto points (i.e., zeros of the Chebyshev polynomials

$$\xi_j = \cos\frac{\pi j}{M}, \quad \eta_k = \cos\frac{\pi k}{N},$$

$$j = 0, ..., M; k = 0, ..., N,$$

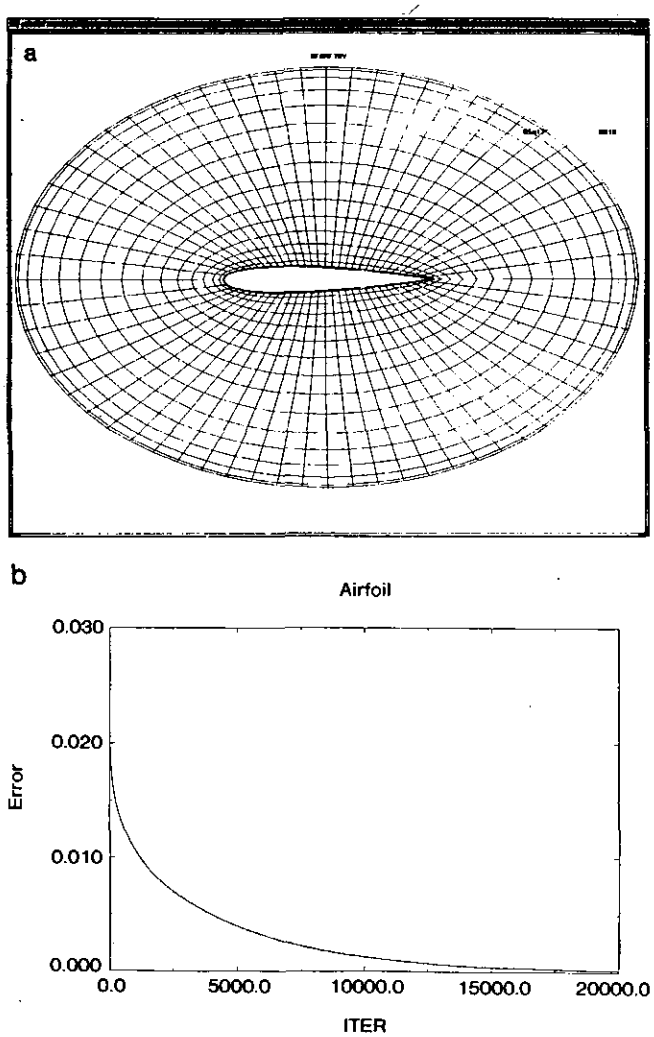

FIG. 5. (a) Coordinates around a NACA0012 airfoil with an ellipse as the outer boundary. (b) Error decrement behavior in the parameter stepping procedure used in obtaining the coordinates in Fig. 5a.

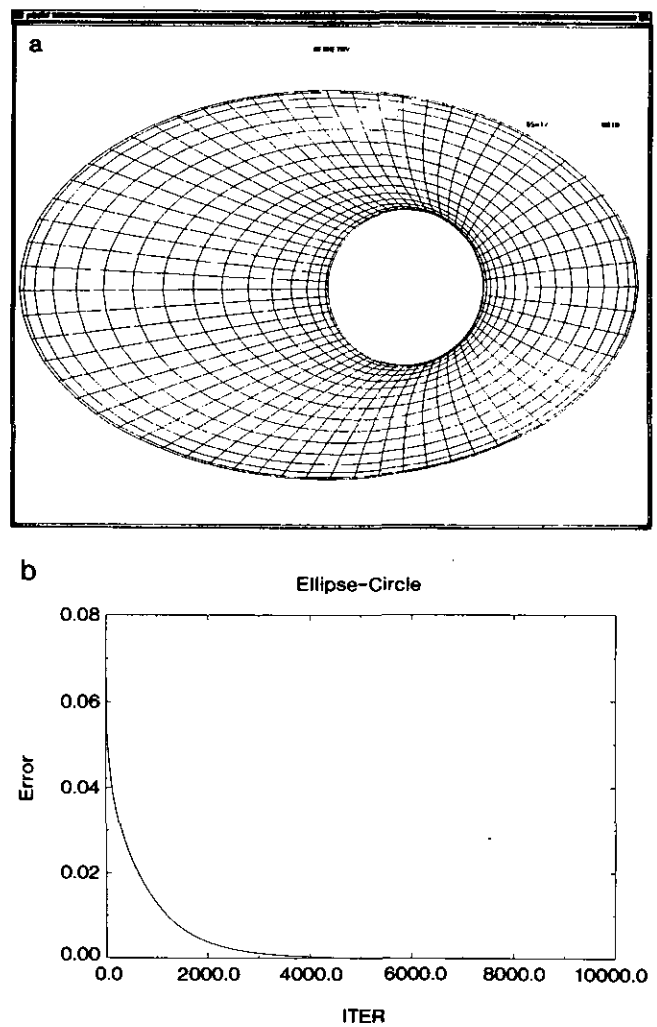

FIG. 6. (a) Coordinates generated between non-concentric circle and ellipse. (b) Error decrement behavior in the parameter stepping procedure used in obtaining the coordinates in Fig. 6a.

and for the Fourier–Chebyshev method, the nodes in the periodic coordinate ξ are uniform and given by

$$\xi_j = \frac{2\pi j}{N}, \quad j = 0, ..., N-1.$$

Since the boundary values are needed at the quadrature nodes, the boundary data is first used to fit parametric spline on each curve, e.g., the B-spline. From this, the initial grid point coordinates are obtained at the Gauss–Lobatto points. After this operation, the following steps are followed:

a. Using the boundary point data form an initial guess for $\mathbf{r}_{ij}$ in the domain.

b. Calculate $\hat{\mathbf{a}}_{mn}^{(0)(0)}$ through Eq. (4.2b).

c. Use Eq. (3.6) for obtaining the values of $\hat{\mathbf{a}}_{mn}^{(0)(0)}$ at the next parameter level $\sigma + \Delta\sigma$.

d. Find $\mathbf{r}_{ij}$ in the field using Eq. (4.2a).

e. With the $\mathbf{r}_{ij}$ of the domain available from step (d), together with the $\mathbf{r}_{ij}$ at the boundary, go to step (b).

f. Repeat steps (b)–(e) and stop at convergence.

Figures 2a and 3a show the grids for simply connected regions of arbitrary concave–convex boundary lines and of a rotor of a gas turbine. Here the Chebyshev polynomials are used in both the ξ and η directions as they are non-periodic in both directions. Figures 2b and 3b show their convergence rates. Figures 4 and 5a–7a show the grid lines for doubly connected domains, where we have used the Fourier expansion along the periodic ξ-coordinate. Figures 5b–7b show respectively the trend of error decrement. In the case of surface grids shown in Fig. 8a and 9a, we have generated grids only for the simply connected case. Figures 8b and 9b respectively show the trend of error decrement.

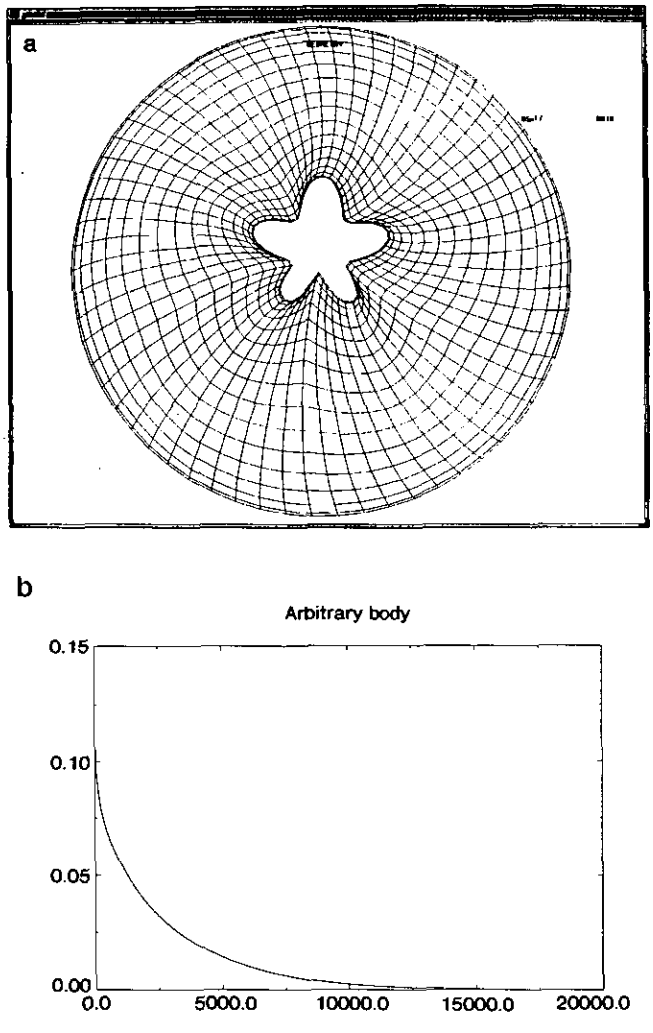

FIG. 7. (a) Coordinates between the inner curve define by $x = r\cos\vartheta$, $y = r\sin\vartheta$, $r = 0.45 + 0.1\sin\vartheta + 0.15\sin 5\vartheta$, and the outer circle $x = 2\cos\vartheta$, $y = 2\sin\vartheta$. (b) Error decrement behavior in the parameter stepping procedure used in obtaining the coordinates in Fig. 7a.

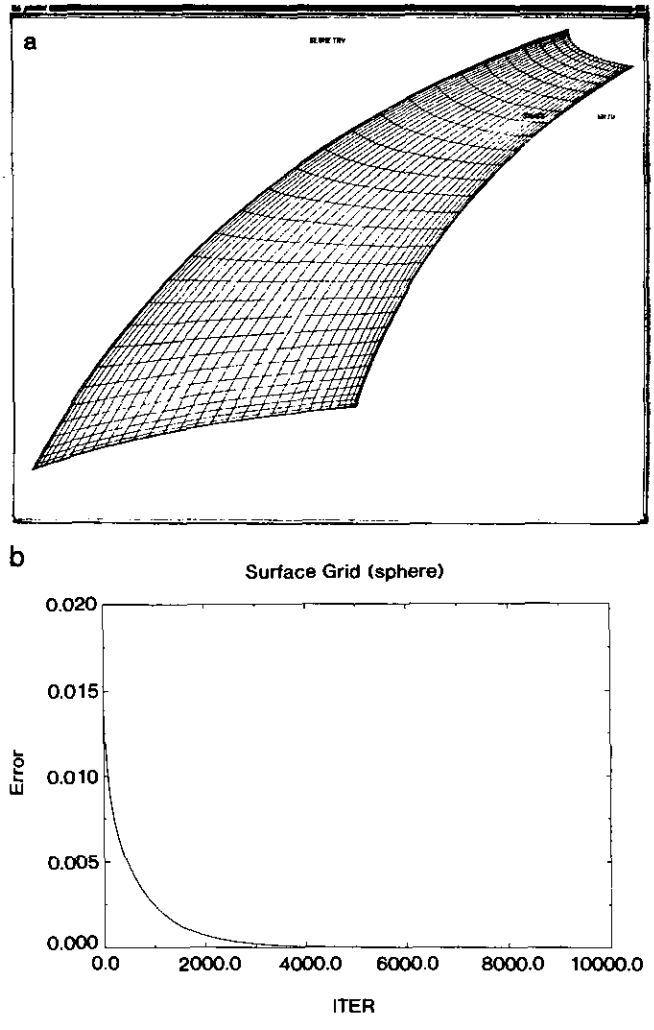

FIG. 8. (a) Coordinates in a patch on the surface of a sphere bounded by $\pi/12 \leqslant \theta \leqslant \pi/3$ and $\pi/6 \leqslant \phi \leqslant 5\pi/12$; θ, ϕ—spherical coordinates. (b) Error decrement behavior in the parameter stepping procedure used in obtaining the coordinates in Fig. 8a.

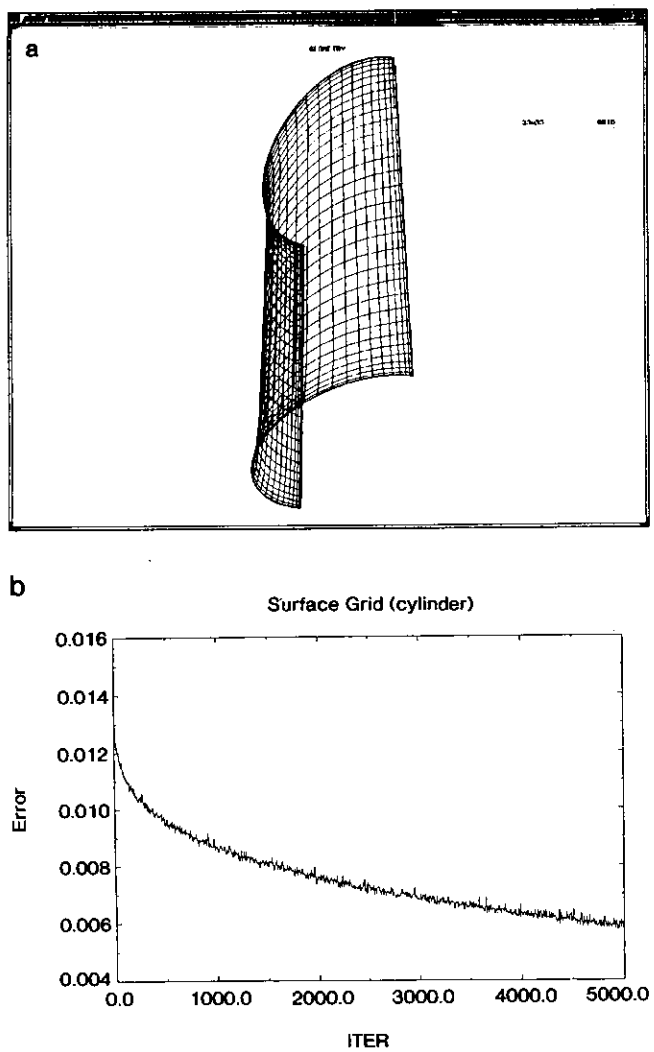

FIG. 9. (a) Coordinates on the surface of an elliptic cylinder. (b) Error decrement behavior in the parameter stepping procedure used in obtaining the coordinates in Fig. 9a.

All the cases tried here have a converging solution with $\Delta\sigma = 10^{-4}$ although the behavior of convergence rate is different for different geometries (see Fig. 5b–7b). For some geometries, the convergence rate shows small wiggles (Figs. 3b and 9b); however, in all cases, there is a monotone reduction of error towards a mean convergence.

V. CONCLUSIONS

In this paper, the method of "parameter stepping" has been used to generate curvilinear coordinates and grid points by using spectral techniques. With the availability of this methodology, it will now become possible to investigate the spectral solution of physical problems, particularly of the nonlinear fluid flow problems, in arbitrary domains.

APPENDIX A

Most of the theory on Chebyshev polynomials is available in Fox and Parker [12] and Rivlin [13]. A collection of usable formulae on Chebyshev polynomials is available in Ref. [2] and in the papers by Gardner *et al.* [14] and Orszag [15]. In this appendix, we have collected those formulae which are of immediate use in the derivations of the equations in Section III.

The Chebyshev polynomials of the first kind of degree n are denoted by $T_n(x)$ in the range $-1 \leqslant x \leqslant 1$ and are simply given by

$$\begin{aligned} T_n(x) &= \cos n\theta \\ x &= \cos\theta. \end{aligned} \tag{A.1}$$

Direct substitution of (A.1) in the equation given below shows that $T_n(x)$ are the solutions of the singular Sturm–Liouville problem

$$-\frac{d}{dx}\left(p\frac{du}{dx}\right) + qu - n^2 wu = 0,$$

with

$$p(x) = (1-x^2)^{1/2}, \quad q(x) = 0, \quad w(x) = (1-x^2)^{-1/2}.$$

Using the trigonometric expansion of

$$\cos(n+1)\theta + \cos(n-1)\theta$$

and (A.1), one easily obtains the recursive formula

$$T_{n+1}(x) - 2xT_n(x) + T_{n-1}(x) = 0, \qquad n \geqslant 1. \tag{A.2}$$

Having $T_0(x) = 1$, $T_1(x) = x$, one can generate Chebyshev polynomials of any desired degree from (A.2).

Equation (A.2) is valid for $n \geqslant 1$. To have an equation valid for $n \geqslant 0$, we introduce the quantities c_m and d_m as follows (cf. [14]):

$$\begin{aligned} &c_o = 2, \quad c_m = 1, \quad m > 0, \\ &d_m = 1, \quad m \geqslant 0, \\ &c_m = 0, \quad d_m = 0, \quad m < 0. \end{aligned} \tag{A.3}$$

Thus, (A.2) is rewritten as

$$2xT_n(x) = c_n T_{n+1}(x) + d_{n-1}T_{n-1}(x), \quad n \geqslant 0. \tag{A.4}$$

From (A.1) it is easy to see that

$$T_n'(x) = n(1-x^2)^{-1/2}\sin n\theta. \tag{A.5}$$

Thus, using the trigonometric expansion of $\cos(n+1)\theta$ and (A.1) and (A.5), we obtain

$$(1-x^2)\,T_n'(x)=n[xT_n(x)-T_{n+1}(x)],\quad n\geqslant 0. \tag{A.6}$$

Using (A.2), the other forms are

$$(1-x^2)\,T_n'(x)=n[T_{n-1}(x)-xT_n(x)],\qquad n\geqslant 1 \tag{A.7}$$

$$=\frac{n}{2}\,[T_{n-1}(x)-T_{n+1}(x)],\quad n\geqslant 1 \tag{A.8}$$

Starting from (A.1), we have

$$T_{n+1}(x)=\cos(n+1)\theta,\quad T_{n-1}(x)=\cos(n-1)\theta.$$

On differentiation with respect to x, we obtain

$$\frac{T_{n+1}'(x)}{n+1}-\frac{T_{n-1}'(x)}{n-1}=2T_n,\quad n\geqslant 1. \tag{A.9}$$

To make (A.9) valid for $n\geqslant 0$, we use (A.3) and have

$$\frac{c_n}{n+1}\,T_{n+1}'(x)-\frac{d_{n-2}}{n-1}\,T_{n-1}'(x)=2T_n(x),\quad n\geqslant 0. \tag{A.10}$$

Orthogonality. The Chebyshev polynomials (functions) form an orthogonal basis. That is, the scalar product of $T_m(x)$ and $T_n(x)$ with weight $w=(1-x^2)^{-1/2}$ is

$$\langle T_m(x),\,T_n(x)\rangle_w=0,\qquad \text{if}\quad m\neq n.$$

To arrive at this result, we start from the integral

$$\int_{-\pi}^{\pi}\cos m\theta\cos n\theta\,d\theta=0\qquad \text{if}\quad m\neq n,$$

$$=\pi\qquad \text{if}\quad m=n\neq 0,$$

$$=2\pi\qquad \text{if}\quad m=n=0.$$

Combining all the three alternatives and noting that the integrand is an even function, we obtain

$$\int_0^{\pi}\cos m\theta\cos n\theta\,d\theta=\frac{\pi}{2}\,c_n\delta_{mn}, \tag{A.11}$$

where $c_0=2$ and $c_n=1$ for $n\geqslant 1$ (refer to (A.3)). From (A.11), we obtain

$$\langle T_m(x),\,T_n(x)\rangle_w=\int_{-1}^{1}(1-x^2)^{-1/2}\,T_m(x)\,T_n(x)\,dx$$

$$=\frac{\pi}{2}\,c_n\delta_{mn}, \tag{A.12}$$

which is the orthogonality property of the Chebyshev functions.

Derivative formulae. Suppose

$$f(x)=\sum_{n=0}^{\infty}a_n^{(0)}T_n(x),$$

then its mth derivative is

$$f^{(m)}(x)=\sum_{n=0}^{\infty}a_n^{(m)}T_n(x).$$

Obviously,

$$\frac{d}{dx}\sum_{n=0}^{\infty}a_n^{(m-1)}T_n(x)=\sum_{n=0}^{\infty}a_n^{(m)}T_n(x).$$

Using (A.10), we obtain

$$\sum_{n=0}^{\infty}a_n^{(m-1)}T_n(x)=\frac{1}{2}\sum_{n=0}^{\infty}\frac{a_nc_n^{(m)}}{n+1}\,T_{n+1}(x)-\frac{a_nd_{n-2}^{(m)}}{n-1}\,T_{n-1}(x).$$

Equating the coefficients of $T_n(x)$ for $n\geqslant 1$, we obtain

$$c_{n-1}a_{n-1}^{(m)}-a_{n+1}^{(m)}=2na_n^{(m-1)},\ n\geqslant 1. \tag{A.13}$$

Repeated application of (A.13) for each m, yields, e.g.,

$$c_na_n^{(1)}=2\sum_{\substack{p=n+1\\ p+n\ \text{odd}}}^{\infty}pa_p^{(0)},\quad n\geqslant 0, \tag{A.14}$$

$$c_na_n^{(2)}=\sum_{\substack{p=n+2\\ p+n\ \text{even}}}^{\infty}p[p^2-n^2]\,a_p^{(0)},\quad n\geqslant 0. \tag{A.15}$$

APPENDIX B: NOMENCLATURE

$\mathbf{a}_{mn}^{(p)(q)}$	Spectral coefficients in the continuous representation.
$\hat{\mathbf{a}}_{mn}^{(p)(q)}$	Spectral coefficients in the discrete representation.
c	Constant introduced in Eq. (2.2)
c_n	2 if $n=0$, otherwise 1.
g	$\det(g_{ij})$.
g_{ij}, g^{ij}	Covariant and contravariant metric coefficients
G_3	$g_{11}\,g_{12}-(g_{12})^2$, appearing in surface theory.
$k_I^{(\nu)}+k_{II}^{(\nu)}$	Twice the means curvature of a surface defined as $x^\nu=\text{const.}$
$\mathscr{L}$	Differential operator; Eqs. (2.4), (2.9).
$\mathbf{n}^\nu$	Unit surface normal vector on $x^\nu=\text{const.}$
P_{ij}^k or $P_{\alpha\beta}^{\delta}$	Control functions.

P^k	Control functions formed by a linear combination of P_{ij}^k; (2.5b); $k = 1, 2, 3$, or $k = 1, 2$.
R	$(k_I^{(v)} + K_{II}^{(v)})\, G_v$.
$\mathbf{r}$	(x, y, z).
$\mathbf{r}_{jk}$	Coordinates x_{jk}, y_{jk}, z_{jk} at grid location j, k.
$\mathbf{r}_{,i}$	$\partial \mathbf{r}/\partial x^i$, $\mathbf{r}_{,ij} = \partial^2 \mathbf{r}/\partial x^i\, \partial x^j$, etc.
$\mathbf{r}_\xi$	$\partial \mathbf{r}/\partial \xi$, $\mathbf{r}_{\xi\eta} = \partial^2 \mathbf{r}/\partial \xi\, \partial \eta$, etc.
x^i	3D curvilinear coordinates.
x^a	Curvilinear coordinates in a surface.

Note. In Section II, summation convention on repeated upper and lower indices has been used.

REFERENCES

1. D. Gottlieb and S. A. Orszag, *Numerical Analysis of Spectral Methods: Theory and Applications* (SIAM-CBMS, Philadelphia, 1977).
2. C. Canuto, M. Y. Hussaini, A. Quarteroni, and T. A. Zang, *Spectral Methods in Fluid Dynamics* (Springer-Verlag, New York, 1988).
3. S. A. Orszag, *J. Comput. Phys.* **37**, 70 (1980).
4. G. P. Koomullil, Ph.D. dissertation, Mississippi State University, December 1991.
5. J. F. Thompson, F. C. Thames, and C. W. Mastin, *J. Comput. Phys.* **15**, 299 (1974).
6. J. F. Thompson, Z. U. A. Warsi, and C. W. Mastin, *Numerical Grid Generation: Foundations and Applications* (North-Holland, Amsterdam/New York, 1985).
7. H. B. Keller, in *Numerical and Physical Aspects of Aerodynamic Flows*, edited by T. Cebeci (Springer-Verlag, New York, 1982), p. 3.
8. Z. U. A. Warsi, *J. Comput. Phys.* **64**, 82 (1986).
9. Z. U. A. Warsi, *Appl. Math. Comput.* **21**, 295 (1987).
10. Z. U. A. Warsi, *AIAA J.* **19**, 240 (1981).
11. Z. U. A. Warsi and G. P. Koomullil, in *Numerical Grid Generation in Computational Fluid Dynamics and Related Fields*, edited by A. S. Arcilla *et al.* (North-Holland, Amsterdam, 1991), p. 955.
12. L. Fox and I. B. Parker, *Chebyshev Polynomials in Numerical Analysis* (Oxford Univ. Press, London, 1968).
13. T. J. Rivlin, *The Chebyshev Polynomials* (Wiley, New York, 1974).
14. D. R. Gardner, S. A. Trogdon, and R. W. Douglass, *J. Comput. Phys.* **80**, 137 (1989).
15. S. A. Orszag, *J. Fluid Mech.* **50**, 689 (1971).